Tensile-strained GaAs quantum wells and quantum dots in a $GaAs_xSb_{1-x}$ matrix

A. A. Toropov, O. G. Lyublinskaya, B. Ya. Meltser, V. A. Solov'ev, A. A. Sitnikova, M. O. Nestoklon, O. V. Rykhova, and S. V. Ivanov
A.F. Ioffe Physico-Technical Institute, Russian Academy of sciences, St. Petersburg 194021, Russia

K. Thonke and R. Sauer
Abteilung Halbleiterphysik, Universität Ulm, 89081 Ulm, Germany
(Received 6 April 2004; revised manuscript received 24 August 2004; published 10 November 2004)

We report on the fabrication and analysis of tensily strained thin GaAs layers ("insertion layers") in a $GaAs_xSb_{1-x}$ matrix ($x<0.05$). The GaAs insertion layers vary in nominal thickness in the range of 0.6–2 monolayers. They were grown by molecular beam epitaxy on GaSb substrates. Transmission electron microscopy studies indicated either growth of ultra-thin quantum wells (QWs) or self-organized formation of quantum dots (QDs), depending on the nominal thickness of the insertion layers. Two photoluminescence (PL) peaks are observed at photon energies below the $GaAs_xSb_{1-x}$ band edge. One of them, detected near 0.7 eV for any insertion layer thickness, is attributed to the emission of a type II QW. The second peak shifted toward smaller energies in the thicker insertion layers is assigned to the PL of type II QDs. This assignment is supported by microscopic tight-binding calculations of the QW electron states.

DOI: 10.1103/PhysRevB.70.205314 PACS number(s): 73.22.−f, 78.55.Et, 78.67.−n

I. INTRODUCTION

The Ga(As,Sb) material system has recently attracted much attention due to a variety of self-organization phenomena such as ordering, clustering, and spontaneous compositional modulation in solid alloys as well as strain-induced formation of quantum dots (QDs). These phenomena result both in compositional features within the GaAsSb bulk layers[1–3] and quantum wells (QWs),[4] and in the formation of GaSb QDs in a GaAs matrix.[5–9] Among the potential device applications of the QW structures are optoelectronic devices[10–12] and ultra-fast all-optical polarization switches,[13] whereas the type II QDs may prove to be useful in carrier storage devices.[14,15]

Recently, we have proposed and fabricated by molecular beam epitaxy (MBE) a type of Ga(As,Sb) nano-structures incorporating thin GaAs insertion layers in a GaSb matrix.[16] The samples with either a single GaAs insertion layers or a GaAs/GaSb superlattice showed bright photoluminescence (PL) below the GaSb band gap. This was attributed to type II transitions between electrons confined in the tensily strained GaAs and holes in the surrounding GaSb. Furthermore, cross-sectional transmission electron microscopy (TEM) images clearly demonstrated the strain-induced formation of QDs when the GaAs layer thickness exceeded 1–1.5 monolayers (ML).[16]

A specific feature of these GaAs QDs is a smaller lattice constant with respect to the GaSb substrate (the lattice mismatch between GaAs and GaSb is ~7.5%). Therefore the structures are tensily strained. This is in contrast to the QD heterostructures studied before (InAs/GaAs,[17] (Ga,In,Al)Sb/GaAs,[5,7] InAs/InP,[18] InP/InGaP,[19] and InP/GaAs[20,21]), where the driving force of the QD formation is the compressive strain. To the best of our knowledge, only one example of self-assembled tensily strained GaAs and AlAs nanoclusters in an InAs matrix has been reported so far.[22] However, these clusters have no confined electron or hole states because the (Ga,Al)As/InAs band line-ups are of type I and the band gaps of GaAs and AlAs are larger than that of InAs. In the type II QDs there is always a confined level at least for one type of carrier, no matter how large the band gaps of the constituent materials. Therefore a GaAs QD in a GaSb matrix is a unique object, where the peculiarities of the QD formation driven by the tensile strain can be studied by means of PL spectroscopy. The analogous situation, when the insertion layers of a wider-band-gap material results in a PL peak below the band gap of a narrower-band-gap matrix was previously observed for a thin AlAs insertion layer in a GaSb matrix, due to the type II band line-ups at the AlAs/GaSb heterointerface.[23] Possible applications of the GaAs-in-GaSb nanostructures can be in the field of $2-3\ \mu$m range mid-IR optoelectronics. Besides, the type II QD structures might be of interest for spintronic applications, especially for spin storage devices, due to their expected long carrier lifetimes and long electron spin relaxation times.[24]

In this paper we report on detailed structural and optical studies of GaAs thin QWs and QDs in a $GaAs_xSb_{1-x}$ matrix with a small content of As ($x<0.05$). The studied samples, fabricated by MBE, differed in the matrix composition, GaAs nominal thicknesses, and growth regimes. X-ray diffraction (XRD) and TEM studies were performed to analyze the structure morphology and composition. PL spectra were measured as a function of the excitation power and temperature, providing information on the electronic states of the nanostructures. For some samples, the substrate rotation was stopped during the growth of the GaAs insertion layer, resulting in a lateral thickness gradient. Position dependent PL studies in such graded samples allowed us to separate the emission originating from the type II transitions in the GaAs nanostructures and the PL features caused by the carrier recombination in the tensily strained $GaAs_xSb_{1-x}$ matrix. The assignment of the PL peaks was supported by a tight-binding

calculation of the electron localization energy in the ultrathin GaAs insertion layers. Both TEM and PL studies give evidence for the formation of type II QDs with zero-dimensional (OD) density of states in the structures with thick enough GaAs insertion layers.

II. EXPERIMENT

A. Sample fabrication

All samples were grown on (001) oriented GaSb substrates at 520 °C using a Riber 32 MBE set up. Conventional effusion cells were used for Ga and Al. Two different configurations were employed for the volatile components (arsenic and antimony). A number of structures (type A samples) were grown with a conventional effusion cell of As, providing a beam of As_4 molecules, and a valveless cracker source of Sb_2 molecules (RB-075-Sb). Other samples (type B) where grown using an As cracker valve cell (VAC 500) and a standard effusion cell for generating a beam of Sb_4 molecules. The temperature of the cracking zone of the As valve cracker cell was chosen low enough to provide the dominating flux of As_4 molecules that suppresses significantly the Sb-As exchange reactions on the GaSb surface. The sample surfaces were monitored *in situ* using a reflection high energy electron diffraction (RHEED) system.

A 0.5 μm thick GaSb buffer was deposited prior to the growth of the structure. The structure was designed so as to incorporate a 0.2–0.3 μm thick layer of $GaAs_xSb_{1-x}$ sandwiched between 20–30 nm thick $Al_{0.5}Ga_{0.5}Sb$ barriers. These barriers were grown to confine photoexcited carriers and, hence, to enhance the PL efficiency. A single GaAs insertion layer was centered within the $GaAs_xSb_{1-x}$ layer. A (2×4) surface reconstruction pattern was observed by RHEED during the growth of GaAs giving evidence for an As-stabilized growth. Substrate rotation was stopped for some samples during the growth of the GaAs insertion layer. This resulted in a lateral thickness gradient of the insertion layer due to the gradient of the Ga flux. Growth was interrupted for 2 and 10 s, respectively, before and after growing the insertion layer. The samples differed in the As content (x) in the $GaAs_xSb_{1-x}$ layer and in the nominal thickness of the GaAs insertion layer.

B. Structural characterization

Figure 1 shows $\Theta-2\Theta$ XRD rocking curves measured near the (004) reflex of an "empty" (i.e., without an insertion layer) type B sample with a $GaAs_{0.05}Sb_{0.95}$ layer (a), a type B sample with a graded-thickness GaAs insertion layer in a $GaAs_{0.02}Sb_{0.98}$ matrix (b), and a type A sample with a graded-thickness GaAs insertion layer in a $GaAs_xSb_{1-x}$ matrix, where x was estimated to be 0.035–0.055 (c). As expected, the rocking curves are not sensitive to the parameters of the thin GaAs insertion layer. On the other hand, the peak due to the reflection from the tensily stressed $GaAs_xSb_{1-x}$ layer is observed in the range of $0<\Theta<1000$ arc sec. Thickness oscillations are also visible in all rocking curves, confirming the perfect flatness of the structures. Note that the peak from $GaAs_xSb_{1-x}$ is broader and less perfect shaped in the type A sample, reflecting most probably a certain compositional inhomogeneity of the layer. Therefore the determination of the $GaAs_xSb_{1-x}$ layer composition is less accurate in this case. This is typical for all samples of type A studied. The compositional inhomogeneity could result from the noticeable As incorporation (1–3%) due to the quite high As background pressure even for closed-shutter growth. Gradual increase of the As cell temperature before the growth of GaAsSb results in a change of the As background pressure and, hence, in the formation of a GaAsSb alloy with a compositional gradient along the growth axis instead of the top part of the GaSb buffer layer. The unintentional As incorporation has also prevented the growth of the samples with a pure GaSb matrix. As for the type B samples, such unintentional incorporation of arsenic was prevented by the use of a valve As source. The most consistent set of TEM and optical data discussed further in the paper was obtained from the type A sample, for which the XRD rocking curve is shown in Fig. 1(c). The type B samples with precisely determined composition of GaAsSb were especially useful for identification of the optical transitions originating from the GaAsSb matrix, as discussed in Sec. III of the paper.

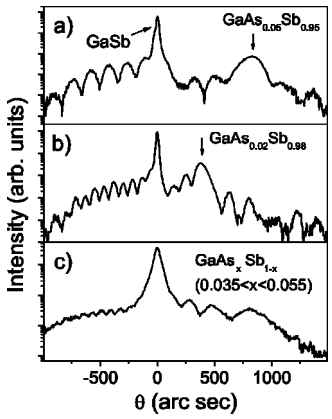

FIG. 1. (004) reflection XRD rocking curves measured in a type B sample without any insertion in the $GaAs_{0.05}Sb_{0.95}$ matrix (a), a type B sample with a graded thickness GaAs insertion in the $GaAs_{0.02}Sb_{0.98}$ matrix (b), and a type A sample with a graded thickness GaAs insertion in the $GaAs_xSb_{1-x}$ matrix with $0.035<x<0.055$ (c).

TEM studies were performed using an EM-420 Philips microscope operating at 100 keV. The specimens for TEM were prepared using cross-section and plan-view thinning in a Gatan 600 ion mill. The images were obtained from the type A sample at different successive points of the wafer along the direction of the GaAs thickness gradient. Closely neighboring sample points were used for measuring PL spectra, as will be discussed below. Figures 2(a)–2(d) present electron micrographs of the sample cross section, imaged at (020) two-beam conditions. The values of the nominal GaAs thickness, shown in the plots, were estimated according to the previously performed calibrations of the growth rate at the sample center and the estimated gradient of the flux along the sample surface. The images of the thinnest layers [Figs. 2(a) and 2(b)] reveal an ultra-thin uniform stripe. The insertion layer in Fig. 2(c) still preserves the flat geometry,

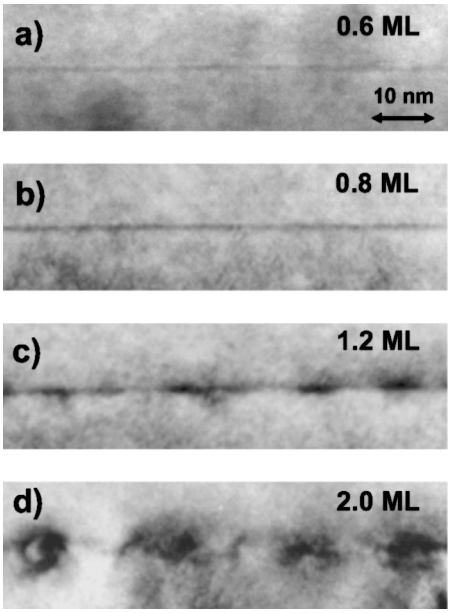

FIG. 2. Cross-section TEM images of a GaAs insertion with different nominal thicknesses: 0.6 ML (a), 0.8 ML (b), 1.2 ML (c), and 2.0 ML (d).

but the morphology is rougher and the formation of islands is obvious. Both the lateral size and height of the islands in this image are distorted by the strain contrast. However, their average sizes can be estimated as not exceeding 6 nm (diameter) and 1 nm (height). An increase in the nominal thickness of a GaAs insertion up to 1.5–2.0 ML results in the formation of 3D clusters accompanied by dislocation loops [see Fig. 2(d)]. Figure 3 depicts a plan-view image of the GaAs islands, taken along [001] at a spot of the wafer close to the one shown in Fig. 2(c). This image allows more accurate measurements of the lateral islands sizes. The histogram in Fig. 3 shows the lateral size distribution of the islands, which peaks near 6 nm in accordance with the cross-section image in Fig. 2(c). The island sheet density can be estimated from this image to be no less than $\sim 4\times 10^{10}$ cm^{-2}.

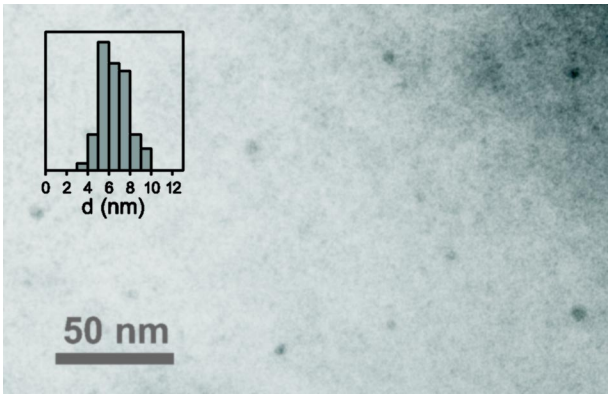

FIG. 3. Plan-view TEM image of islands formed within the 1.2 ML thick GaAs insertions. The inset shows the lateral size distribution of the islands.

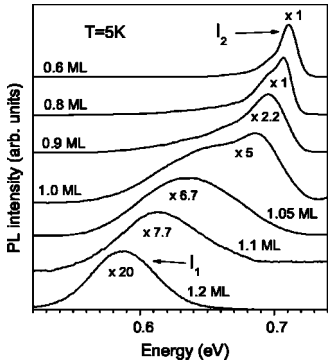

FIG. 4. PL spectra measured at successive points along the gradient direction in a type A sample with graded thickness. The respective GaAs nominal thicknesses are marked at each curve. The spectra are multiplied by the factors given at the curves and are arbitrarily offset.

C. Photoluminescence studies

PL spectra were measured in a variable temperature He cryostat in the range of 4.5–300 K. They were excited by the 532 nm line of a frequency-doubled Nd:YAG *cw* laser or the 809 nm line of an injection laser diode. The excitation spot size on the sample was in the range of 0.2–0.5 mm. Either a Bomem Fourier transform infrared spectrometer with a nitrogen-cooled InAs photodiode or a grating monochromator with a PbS photoresistor were used for the detection of the PL signals.

We present here mainly PL data of the particular type A sample. The PL spectra of type B samples are in general similar. Figure 4 shows a number of low-temperature PL spectra measured with excitation by the 809 nm laser line with a power density of 3 W/cm^2. The spectra were measured at successive points along the direction of the GaAs thickness gradient. They clearly depend on the measurement position. There is a relatively narrow PL peak at ~0.7 eV in the samples with thin enough insertion layers (less than ~1 ML), labeled I_2 in Fig. 4, with two weak LO phonon replicas. A wider peak (I_1) emerges in the thicker layers (between 1.0 and 1.2 ML) at lower energy. The two peaks coexist in the spectrum only in a very narrow range of nominal GaAs thickness. In the samples with an even thicker insertion layer, peak I_2 disappears while peak I_1 shifts to lower energies, decreases in intensity, and finally disappears as well. These findings suggest that the I_1 and I_2 PL peaks can be ascribed to the intrinsic emission of the GaAs insertion layer. Moreover, the appearance of I_1 correlates with the emergence of QDs in the TEM images (see Fig. 2). This leads us to attribute it to QD emission.

Figures 5(a)–5(c) show the temperature dependence of the PL spectra measured at three different spots corresponding to "thin" [0.8 ML, Fig. 5(a)], "intermediate" [1.05 ML, Fig. 5(b)], and "thick" [1.2 ML, Fig. 5(c)] GaAs insertion layers. For demonstrative purposes all the spectra are normalized and vertically offset. With increasing temperature the I_2 peak intensity in Fig. 5(b) is enhanced. Furthermore, two additional peaks appear in the spectra in Figs. 5(a) and 5(b), following the temperature-induced increased population of

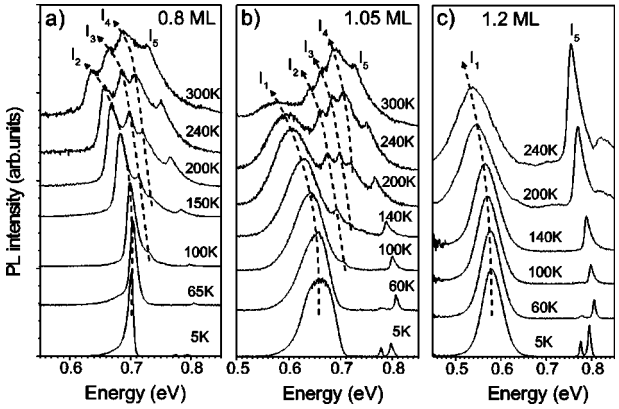

FIG. 5. Temperature dependent PL spectra measured at an excitation power density of 10 W/cm^2 (532 nm laser line) in a graded thickness type A sample at three points with different nominal GaAs thicknesses: 0.8 ML (a), 1.05 ML (b), and 1.2 ML (c). For clarity the spectra are arbitrarily offset and normalized. Dashed lines are eye guides.

the higher-energy states. These peaks are labeled I_3 and I_4. Their energy positions are practically independent of the insertion layer thickness. Such peaks were also observed in the reference sample grown without a GaAs insertion layer, hence, they can be attributed to emission from the GaAsSb matrix. The successive activation of the I_2-I_4 peaks at higher temperatures relative to I_1 confirms that all luminescent states belong to the same electronic system being in thermal quasiequilibrium. This system is apparently the GaAs insertion layer with the surrounding GaAsSb matrix. In the thickest insertion layers [Fig. 5(c)] the energy difference between I_1 and I_2 is so large that the I_2-I_4 peaks are not visible under the relatively low excitation power up to the highest temperature. The I_5 peak observed at higher energy is close to the band-gap energy of pure GaSb. This peak is assigned to the emission of the buffer layer. Such attribution means that most parts of the buffer layer, grown before switching on the As effusion cell, does not suffer from the unintentional incorporation of arsenic. All PL features shift with increasing temperature to lower energies, following the band gap shrinkage.

The excitation power dependence of the low-temperature PL spectrum is illustrated in Fig. 6 showing the I_1 (a) and I_2 (b) PL spectra at different excitation powers. Fig. 6(a) corresponds to a nominal insertion layer thickness of 1.2 ML, and Fig. 6(b)-to a nominal thickness 0.8 ML. Figure 7 shows the peak energy positions (a) and full widths at half maximum (FWHM) (b) for I_1 (open circles) and I_2 (solid squares) versus excitation power density. With the increase of excitation power, both peaks noticeably shift to higher energies. For the I_1 peak, the shift is accompanied by an increase in FWHM, mainly due to a peak broadening toward higher energies. For the I_2 peak a relatively narrow major component is observed, which slowly upshifts in energy with excitation. At low excitation densities a presumably defect-related, saturable low-energy component is additionally observed. In Fig. 6(b) the overall linewidth therefore seems to increase for low excitation, while the dominant component actually retains its FWHM.

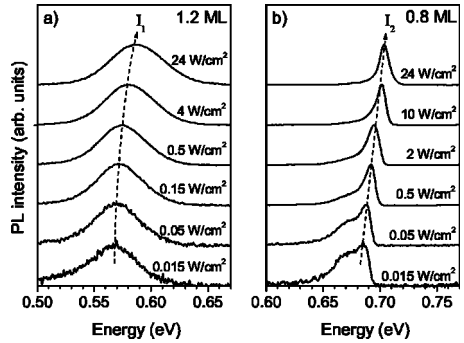

FIG. 6. PL spectra measured at 5 K versus excitation power density (532 nm laser line). Dashed curves are plotted only to guide the eye. The spectra are arbitrarily offset and normalized.

III. DISCUSSION

A. Band energies of the $GaAs_xSb_{1-x}$ matrix

To establish a correlation between the PL spectra and structural features visible in TEM images we first estimate band line-ups for the Ga(As,Sb) system. Furthermore, in the next subsection we will calculate electron confinement energies for a model structure including integer numbers of GaAs monolayers in a GaSb matrix.

Figure 8 displays the relative positions of the conduction band bottom (el) and heavy hole (hh) and light hole (lh) valence band tops for a layer of solid $GaAs_xSb_{1-x}$ alloy grown pseudomorphically on a GaSb substrate, as a function of the As content x. All parameters for the calculation were taken from Ref. 25. Following Van de Walle,[26] the band-gap bowing was completely attributed to the conduction band. Dashed curves present the calculation performed for the unstrained alloy, whereas solid curves correspond to the layer under biaxial stress. The strain splits the valence band so that the light-hole band is higher in energy. Due to both, the large band-gap bowing and the strain effect, an increase in the

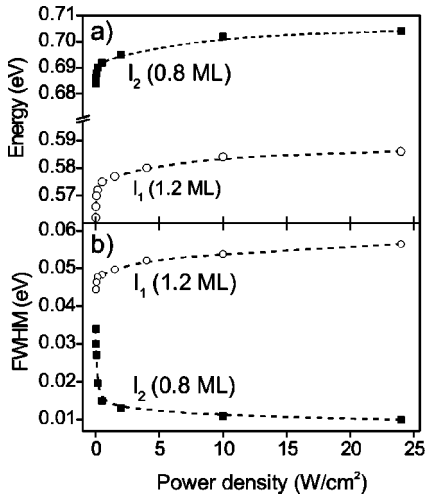

FIG. 7. PL peak energy (a) and full width at half maximum (FWHM) (b) for I_1 (open circles) and I_2 (solid squares) peaks versus excitation power density. Dashed curves are plotted only to guide an eye.

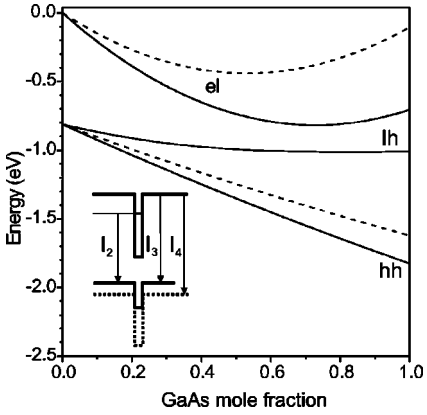

FIG. 8. Relative positions of the conduction band bottom (el) and heavy hole (hh) and light hole (lh) valence band tops for a $GaAs_xSb_{1-x}$ solid alloy. Dashed curves correspond to the unstrained solid alloy, whereas solid curves are relevant to the tensily strained layer grown pseudomorphically on a GaSb substrate. The inset illustrates band line-ups and optical transitions for a type II QW of $GaAs_ySb_{1-y}/GaAs_xSb_{1-x}$ (see text).

GaAs mole fraction results in a band-gap shrinkage in the extended range $0<x<0.73$. In the same range, the $GaSb/GaAs_xSb_{1-x}$ conduction band offset increases for higher As content. It follows from Fig. 8 that the band line-ups at the $GaAs_ySb_{1-y}/GaAs_xSb_{1-x}$ interface ($y>x$) are of type II for both light and heavy holes for any y, provided x is small enough. $GaAs_ySb_{1-y}$ is thus a barrier for holes, whereas $GaAs_xSb_{1-x}$ is a barrier for electrons. The band line-ups for a corresponding QW structure and possible optical interband transitions are schematically shown in the inset in Fig. 8. Note that the light-hole band (solid line) is the top-most valence band both in the insertion layer and in the matrix. The heavy-hole band is shown in the inset by a dotted line.

Figure 9 displays the heavy-light hole band splittings versus the As content. The solid line represents the results of the calculation, whereas the circles correspond to the energy spacing between the I_3 and I_4 PL peaks in the measurements for both type B samples (solid circles) and a type A sample (open circle). The $GaAs_xSb_{1-x}$ composition was obtained from XRD measurements. The accuracy of the composition determination was much better for the type B samples, as indicated by horizontal error bars on the plot. The apparent correspondence suggests that the I_3 and I_4 peaks can be attributed to the emission of light- and heavy- hole excitons in the strained $GaAs_xSb_{1-x}$ matrix. The respective transitions are schematically shown in the inset in Fig. 8. Note that in the structures with GaAs insertion layers these transitions are dependent on the temperature-activated population of the conduction- and heavy-hole bands in the $GaAs_xSb_{1-x}$ matrix. In spite of the lower population, these transitions which are direct in space can be even stronger than the type II transition I_2.

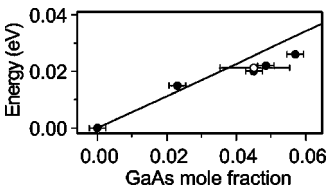

FIG. 9. Strain-induced splitting of heavy- and light-hole bands in a $GaAs_xSb_{1-x}$ solid alloy grown pseudomorphically on a GaSb substrate, versus the As content x. The solid line represents the results of the calculation and circles are from the PL data. Solid circles correspond to type B samples and the open circle represents a type A sample.

B. $GaAs/GaAs_xSb_{1-x}$ quantum dots and thin quantum wells

Direct comparison of the PL spectra (Fig. 4) and TEM images (Fig. 2) led us to assign the I_1 peak to the emission of QDs. Evidence for the 0D nature of the states responsible for the I_1 peak is also provided by the excitation-dependent PL measurements. Both the I_1 and I_2 peaks shift to higher energies with an increase of the excitation power. A similar effect was previously observed for type II QWs (Ref. 27) and type II QDs.[5,21,28] In the case of type II QWs, this shift reflects the formation of a dipole layer caused by the spatial separation of nonequilibrium excess carriers. Recently, it has been demonstrated that in type II QDs the blueshift of the emission band is due to the filling of higher-energy states rather than to a variation of the electrostatic potential.[21,28] The specific feature of the state filling process is the broadening of the emission band. Indeed, a noticeable broadening accompanies the blueshift of the I_1 peak, whereas the spectral width of the higher energy component of the I_2 peak is almost constant (see Figs. 6 and 7). This observation confirms the assignment of the I_1 peak to the QDs emission.

Let us now turn to the origin of the I_2 PL peak. An emission peak between a QD emission line and a PL line from a surrounding matrix was frequently observed in different QD systems. Usually it is attributed to the emission of the so-called "wetting layer," which is a QW connecting QDs in the lateral dimension (see, e.g., Refs. 5 and 17). Such a QW is visible in the TEM images in Fig. 2 even for the insertion layers as thick as 1.2 ML. It seems natural to attribute the I_2 PL peak to the emission from this QW. However, the I_2 peak exhibits untypical behavior, since its position is only weakly dependent on the nominal thickness of the insertion layer. Usually, the position of the emission line from the "wetting layer" efficiently shifts towards lower energies with an increase in the amount of deposited material. In InAs/GaAs QD heterostructures the "wetting layer" PL line shifts down by 50–70 meV with the increase in the InAs nominal thickness from 0.6 to 1.2 ML.[29] In the present case, the observed shift of the I_2 peak is hardly more than 20–30 meV.

To provide an insight into the behavior of the "wetting layer" PL, we have calculated electron states in a thin GaAs QW imbedded in a GaSb matrix. The validity of the envelope function approach is questionable, when dealing with layers as thin as a few MLs. Therefore in addition to the Kane model[30] we have used a microscopic tight-binding approach which should work down to 1 ML QW thickness. For strained GaAs, one may apply the tight-binding method taking into account the strain-induced valence band splitting, like in Ref. 31. However, an analysis carried out in the

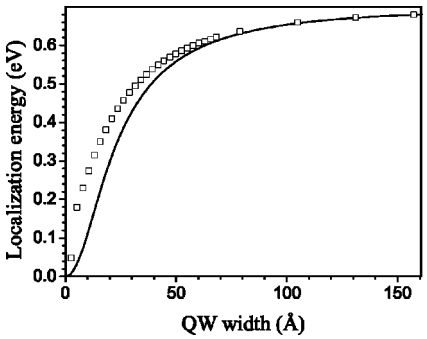

FIG. 10. Electron localization energy for a GaAs QW in a GaSb matrix. The solid curve represents the data obtained within the Kane model. Open squares show the results of the tight-binding calculation, where for low widths each square corresponds to a monolayer step.

framework of the Kane model showed that the inclusion of the hh-lh valence band splitting leads only to minor changes in the energy of the electron states (within a limit of a few percent). This allows us to state that general properties of the electron states in thin QWs are correctly reproduced in the tight-binding theory taking no account of the strain-induced effects in the valence band.

The calculation was performed in the frame of a 20-band tight-binding model including spin-orbit splitting (see Ref. 32 and references therein). It uses sp^3s^* tight-binding parameters chosen so as to reproduce several main features of the fundamental properties of the bulk constituents. For 15 sp^3s^* tight-binding parameters of GaSb we have used the values from Ref. 32. For the parameters of GaAs, there is the problem of very different values for strained and unstrained GaAs, even if one neglects the hh-lh splitting. As a result, for this material we were not able to use any previous fit. Hence, we applied the tight-binding parameters chosen so as to reproduce the effective electron mass and band gap of the strained bulk material. Our analysis showed that variations of the GaAs tight-binding parameters, which leave the general band structure properties unchanged, lead only to minor changes in the electron level positions.

Figure 10 shows the calculated electron localization energy as a function of the QW thickness. The data obtained in the framework of the Kane model are plotted by the solid curve. Squares represent the results of the tight-binding approach, obtained for discrete thicknesses corresponding to multiple MLs. For layers thicker than 10–15 MLs the two methods give comparable results. However, for smaller widths there are significant discrepancies that reflect the failure of the envelope function approximation for the thinnest layers. The most reasonable explanation for such big discrepancies is that the effective mass model neglects the electron-hole mixing at the interfaces, which is allowed by the breakdown of translational invariance. For large electron wave vectors the valence-band admixture can be significant, increasing the electron localization energy.

From Fig. 10 one can conclude that the electron localization energy for a single GaAs ML in GaSb is 48 meV. To compare this result with the PL data one should bear in mind that the QW barriers in the samples consist of a $GaAs_xSb_{1-x}$ solid alloy rather than of pure GaSb as used in the calculation. However, for small x and thin QWs the electron localization energy is practically insensitive to the compositional variation of the solid alloy because the electron level-which is shallow with respect to the barrier potential-does not "feel" the corresponding relatively small variation of the QW depth. Another factor influencing the PL peak energy in a type II QW is the electrostatic band bending induced by the nonequilibrium photo-excited carriers. To avoid this effect one should use the experimental data in the low-excitation limit. In this limit, neglecting the exciton binding energies, the electron localization energy can be approximated by the energy difference between the PL peaks I_2 and I_3 (see the inset in Fig. 8). The value obtained for the insertion layer thicknesses in the range of 0.6–1.0 ML can be estimated as 40–50 meV. They fit perfectly to the electron localization energy obtained within the tight-binding approach for a 1 ML GaAs insertion. Note that the calculated electron localization energy for a 2 ML thick GaAs QW is as large as ~180 meV.

Previous XRD studies of a GaAs/GaSb SL with submonolayer thick GaAs insertion layers showed that the rocking curves can be better simulated assuming alloyed GaAsSb layers rather than integer or fractional monolayers of GaAs.[16] This is in agreement with the reported data on the efficiency of interdiffusion and segregation processes during the epitaxial growth of nanostructures in the GaAsSb system.[33] Also recent high resolution TEM (HRTEM) studies indicated the formation of an alloyed 2 ML thick $GaAs_xSb_{1-x}$ layer instead of the intended growth of a GaSb insertion layer in a GaAs matrix.[34] Bearing in mind all these data, we assume that the submonolayer thick GaAs insertion layers can be considered as an alloyed $GaAs_xSb_{1-x}$ layer rather than a fractional ML of pure GaAs. This assumption does not contradict the observed stability of the I_2 peak position versus the GaAs nominal thickness, because the variation of the $GaAs_xSb_{1-x}$ composition in the range of $0.5<x<1$ causes relatively small changes of the QW conduction band offset (of the order of 100 meV, see Fig. 8), which for the 1 ML insertion result in a variation of the localization energy within ~8 meV.

Intrinsic compositional modulations can emerge within the insertion or in the surrounding $GaAs_xSb_{1-x}$ matrix due to a variety of inherent self-organization phenomena in a $GaAs_xSb_{1-x}$ solid alloy.[1–3] The occurrence of such effects may be indirectly indicated by the complicated shape of the I_2 line in the samples with submonolayer thick insertions [see Fig. 6(b)]. Additional HRTEM studies are needed to elucidate these issues which are beyond the scope of this paper. Here we tentatively ascribe the I_2 PL peak to the emission of an ultra-thin alloyed $GaAs_xSb_{1-x}$ QW.

IV. SUMMARY AND CONCLUSIONS

We have studied MBE growth as well as structural and PL properties of thin tensily strained GaAs insertion layers in a GaAsSb matrix with a small content of As. Bright PL spectra attributed to the intrinsic emission of either type II QW or type II QDs were observed for the range of 0.6–1.2 ML nominal thickness of the GaAs layers.

The thinnest insertion layers (<1 ML) lead to a fairly homogeneous flat layer, whose emission can be ascribed to the PL of a $GaAs_xSb_{1-x}$ ultra-thin QW. Self-organized QD formation was detected by TEM measurements when the nominal thickness of the insertion layer exceeded ~1 ML. An additional PL peak assigned to the QDs emission splits off from the QW emission band in the samples with thicker insertion layers. The QD PL is visible up to a nominal thickness of ~1.5 ML. In this range the QDs appear as relatively thin (~2–5 ML) disks with characteristic lateral dimensions of ~6 nm. Larger relaxed islands were formed within the insertion layers thicker than ~1.5 ML. These islands are not optically active due to the generation of dislocations leading to enhanced non-radiative recombination.

The self-organization process observed here does not match the classical Stranski-Krastanov growth mode (see, e.g., Ref. 17). The specific features are (*i*) smooth onset of the dot nucleation, (*ii*) flat disk shape of the dots, and (*iii*) very efficient QW-to-QDs transport of carriers. These features are better consistent with the self-organized QD growth observed previously in compressively strained CdSe/ZnSe structures.[35] There ZnCdSe disk-like structures are formed within the alloyed ZnCdSe layer produced by the deposition of a CdSe sheet due to interdiffusion and segregation processes. Similar compositional inhomogeneities were also observed in compressively strained GaSb layers in a GaAs matrix with thicknesses below the onset of 3D growth.[34] Like in our case, transition to a 3D growth mode in thicker layers led to large relaxed islands. These examples have allowed us to conclude that the strain sign (either tensile or compressive) does not influence dramatically the QD formation process.

The driving force of the observed self-organization process could be the strain-induced decomposition of the solid alloy.[36] The well known predisposition of the GaAsSb solid alloy to different ordering and clustering phenomena can also be important for the initial QDs nucleation. The details of these processes in thin layers are not clear at present and require additional studies.

ACKNOWLEDGMENTS

This work was partly supported by the Program "Physics of Solid State Nanostructures" of the Ministry of Sciences of the Russian Federation and RFBR. The authors are grateful to D. Solnyshkov and A. Semenov of the Ioffe Institute for XRD measurements and the assistance in the MBE growth, respectively. S.V.I. is grateful to Russian Science Support Foundation.

[1] H. R. Jen, M. J. Cherng, and G. B. Stringfellow, Appl. Phys. Lett. **48**, 1603 (1986).
[2] I. J. Murgatroyd, A. G. Norman, and G. R. Booker, J. Appl. Phys. **67**, 2310 (1990).
[3] Z. Zhong, J. H. Li, J. Kulik, P. C. Chow, A. G. Norman, A. Mascarenhas, J. Bai, T. D. Golding, and S. C. Moss, Phys. Rev. B **63**, 033314 (2001).
[4] S. L. Zuo, Y. G. Hong, E. T. Yu, and J. F. Klem, J. Appl. Phys. **92**, 3761 (2002).
[5] F. Hatami, N. N. Ledentsov, M. Grundmann, J. Böhrer, F. Heinrichsdorff, M. Beer, D. Bimberg, S. S. Ruvimov, P. Werner, U. Gösele, J. Heydenreich, U. Richter, S. V. Ivanov, B. Ya. Meltser, P. S. Kop'ev, and Zh. I. Alferov, Appl. Phys. Lett. **67**, 656 (1995).
[6] C.-K. Sun, G. Wang, J. E. Bowers, B. Brar, H.-R. Blank, H. Kroemer, and M. H. Pilkuhn, Appl. Phys. Lett. **68**, 1543 (1996).
[7] E. R. Glaser, B. R. Bennett, B. V. Shanabrook, and R. Magno, Appl. Phys. Lett. **68**, 3614 (1996).
[8] R. A. Hogg, K. Suzuki, K. Tachibana, L. Finger, K. Hirakawa, and Y. Arakawa, Appl. Phys. Lett. **72**, 2856 (1998).
[9] B. M. Kinder and E. M. Goldis, Appl. Phys. Lett. **73**, 1233 (1998).
[10] R. T Senger, K. K. Bajaj, E. D. Jones, N. A. Modine, K. E. Waldrip, F. Jalali, J. F. Klem, G. M. Peake, X. Wei, and S. W. Tozer, Appl. Phys. Lett. **83**, 2614 (2003).
[11] Y. S. Chiu, M. H. Ya, W. S. Su, T. T. Chen, Y. F. Chen, and H. H. Lin, Appl. Phys. Lett. **81**, 4943 (2002).
[12] T. T. Chen, C. H. Chen, W. S. Su, M. H. Ya, Y. F. Chen, P. W. Liu, and H. H. Lin, J. Appl. Phys. **93**, 9655 (2002).
[13] K. C. Hall, S. W. Leonard, H. M. van Driel, A. R. Kost, E. Selvig, and D. H. Chow, Appl. Phys. Lett. **75**, 4156 (1999).
[14] M. Geller, C. Kapteyn, L. Müller-Kirsch, R. Heitz, and D. Bimberg, Appl. Phys. Lett. **82**, 2706 (2003).
[15] M. Hayne, J. Maes, S. Bersier, V. V. Moshchalkov, A. Schliwa, L. Müller-Kirsch, C. Kapteyn, R. Heitz, and D. Bimberg, Appl. Phys. Lett. **82**, 4355 (2003).
[16] V. A. Solov'ev, A. A. Toropov, B. Ya. Meltser, Ya. V. Terent'ev, R. N. Kyutt, A. A. Sitnikova, A. N. Semenov, S. V. Ivanov, Motlan, E. M. Goldys, and P. S. Kop'ev, Semiconductors **36**, 816 (2002).
[17] A. Madhukar, Q. Xie, P. Chen, and A. Konkar, Appl. Phys. Lett. **64**, 2727 (1994).
[18] H. Marchand, P. Desjardins, S. Guillon, J.-E. Paultre, Z. Bougrioua, R. Y.-F. Yip, and R. A. Masut, Appl. Phys. Lett. **71**, 527 (1997).
[19] N. Carlsson, W. Seifert, A. Petersson, P. Castrillo, M. E. Pistol, and L. Samuelson, Appl. Phys. Lett. **65**, 3093 (1994).
[20] B. Wang and S.-J. Chua, Appl. Phys. Lett. **78**, 628 (2001).
[21] M. K. K. Nakaema, F. Likawa, M. J. S. P. Brasil, E. Ribeiro, G. Medeiros-Ribeiro, W. Carvalho Jr., M. Z. Maialle, and M. H. Degani, Appl. Phys. Lett. **81**, 2743 (2002).
[22] D. A. Tenne, V. A. Haisler, A. I. Toropov, A. K. Bakarov, A. K. Gutakovsky, D. R. T. Zahn, and A. P. Shebanin, Phys. Rev. B **61**, 13 785 (1999).
[23] E. R. Glaser, T. A. Kennedy, B. R. Bennett, and B. V. Shanabrook, Phys. Rev. B **59**, 2240 (1999).
[24] H. Gotoh, H. Ando, H. Kamada, A. Chavez-Pirson, and J. Temmyo, Appl. Phys. Lett. **72**, 1341 (1998).
[25] I. Vurgaftman, J. R. Meyer, and L. R. Ram-Mohan, J. Appl. Phys. **89**, 5815 (2001).
[26] C. G. Van de Walle, Phys. Rev. B **39**, 1871 (1989).

[27] N. N. Ledentsov, J. Böhrer, M. Beer, F. Heinrichsdorff, M. Grundmann, D. Bimberg, S.V. Ivanov, B. Ya. Meltser, S. V. Shaposhnikov, I. N. Yassievich, N. N. Faleev, P. S. Kop'ev, and Zh. I. Alferov, Phys. Rev. B **52**, 14 058 (1995).
[28] L. Müller-Kirsch, R. Heitz, A. Schliwa, O. Stier, D. Bimberg, H. Kirmse, and W. Neumann, Appl. Phys. Lett. **78**, 1418 (2001).
[29] A. S. Bhatti, M. Grassi Alessi, M. Capizzi, P. Frigeri, and S. Franchi, Phys. Rev. B **60**, 2592 (1999).
[30] E. O. Kane, J. Phys. Chem. Solids **1**, 249 (1957).
[31] D. Bertho, J.-M. Jancu, and C. Jouanin, Phys. Rev. B **48**, 2452 (1993).
[32] G. Klimeck, R. C. Bowen, T. B. Boykin, and T. A. Cwik, Superlattices Microstruct. **27**, 519 (2000).
[33] M. Schowalter, A. Rosenauer, D. Gerthsen, M. Grau, and M.-C. Amann, Appl. Phys. Lett. **83**, 4355 (2003).
[34] L. Müller-Kirsch, U. W. Pohl, R. Heitz, H. Kirmse, W. Neumann, and D. Bimberg, J. Cryst. Growth **221**, 611 (2000).
[35] N. Peranio, A. Rosenauer, D. Gerthsen, S. V. Sorokin, I. V. Sedova, and S. V. Ivanov, Phys. Rev. B **61**, 16 015 (2000).
[36] J. Tersoff, Phys. Rev. Lett. **81**, 3183 (1998).